RECONSTRUCTION OF THE VOYAGER 2 NEPTUNE ENCOUNTER IN THE ICRF SYSTEM

Robert A. Jacobson *

Jet Propulsion Laboratory, California Institute of Technology, Pasadena, California 91109

The Neptunian system was visited by the Voyager 2 spacecraft in August of 1989. Data acquired during the encounter led to improved knowledge of the Neptunian satellites' orbits, the mass of the largest satellite, and the mass, gravitational harmonics, and pole orientation of Neptune. To support current and future scientific investigation of the Neptunian system, we have re-examined the Voyager mission taking advantage of improvements made in dynamical and observational modelling and data processing since the earlier analyses. We obtain a revised Voyager trajectory in the International Celestial Reference Frame (ICRF), updated planet and satellite orbits, and an improved Neptunian system gravity field.

I. Introduction

The Neptunian system was visited by the Voyager 2 spacecraft in August of 1989. Refs. 1–3 provide a detailed discussion of the determination of the orbit of the spacecraft. Data acquired during the encounter were subsequently used to improve knowledge of the orbits of the Neptunian satellites, the mass of the largest satellite, Triton, and the mass, gravitational harmonics, and pole orientation of Neptune.[4]

To support current and future scientific investigation of the Neptunian system, we re-examined the Voyager mission. Analogous re-examinations have been done for the Jovian system[5] in connection with the joint analysis of Voyager and Galileo observations, for the Saturnian system[6] in support of joint analysis of Voyager and Cassini observations, and for the Uranian system[7] to facilitate joint analysis of Voyager and Earthbased Uranian ring observations. The objectives of our current work are:

- the determination of the Voyager trajectory in the International Celestial Reference Frame (ICRF);[8] the original Voyager orbit reconstruction was in the B1950/FK4 coordinate system, the standard system adopted for use by the Voyager Project. The ICRF is the reference frame of the current JPL planetary and satellite ephemerides as well as the standard frame of the international astronomical and planetary science community.
- the update of the ephemerides of Neptune and three of its satellites, Triton, Nereid, and Proteus, based on the Voyager observations and all available Earthbased planet and satellite observations.
- a re-investigation of Neptune's gravity field taking advantage of improvements made in dynamical and observational modelling and data processing since the original analysis.

This paper provides a detailed discussion of the reconstruction of the Voyager Neptune encounter trajectory. The work on the satellite orbits will be reported in more depth in a future publication; a brief overview appeared in Ref. 9. The new orbit of Neptune is considered preliminary; it will be superseded by the next JPL planetary ephemeris which will include the Voyager data in its development.

*Member of the Technical Staff, Jet Propulsion Laboratory, Associate Fellow AIAA

II. ANALYSIS

II.A. Data

The original orbit reconstruction[1] spanned the 118 day period from the start of the Observatory phase of the mission on 5 June 1989 to the end of the Post Encounter phase on 1 October 1989. Our work extends the arc backward to the time of the earliest useable imaging data (11 November 1988). The Voyager data set contained:

- noncoherent one-way and coherent two-way and three-way Doppler and two-way and three-way range. These data are the same as those used by in the original reconstruction augmented with data for the period prior to 5 June 1989 from the archival data files. We included additional one-way Doppler during the period of Neptune closest approach; those data were not used previously. Transmission of the radio data carrier to the spacecraft was at S band (2200 MHz); the carrier could be transponded back to the tracking stations at both S band and X band (8400 MHz). However, due to power limitations transponding at both frequencies simultaneously was rarely done. X band was the primary downlink frequency because it provided a higher telemetry rate for science data return. During the encounter, the spacecraft was at low declination and the round trip light time exceeded eight hours. Consequently, two-way tracking was limited to the DSN (Deep Space Network) complex in Australia; three-way Doppler and range became the dominant radiometric data types. We calibrated the data for the effects of the Earth's troposphere and ionosphere. Interplanetary plasma calibrations were unavailable, however, we used a solar corona model to account for plasma induced range delays (the model was developed for Cassini and was not available at the time of Voyager). We also calibrated the three-way data to account for inter-station timing and frequency offsets.[2]
- spacecraft Delta Differential One-way Range (ΔDOR). These data, which are effectively measurements of spacecraft position relative to a nearby quasar, are identical with those used in mission operations.[1] They were calibrated for tropospheric effects; ionosphere calibrations were unavailable, but ionospheric effects tend to cancel in ΔDOR data. We replaced the B1950/FK4 quasar locations with their current ICRF locations.[10] See Ref. 11 and Ref. 12 for a general discussion of ΔDOR data.
- optical navigation imaging (pictures of the satellites against a stellar background). The star locations in these observations were originally referenced to a star catalogue in the B1950/FK4 system; we replaced the locations with ICRF positions from the UCAC2 star catalogue.[13]
- the time of a stellar occultation by Triton recorded by the Voyager ultra-violet spectrometer (UVS) and the time of a radio occultation of the spacecraft by Triton observed during the encounter. These occultations were used in the original Voyager reconstuction. For the stellar occultation, as with the Voyager imaging data, we replaced the original B1950/FK4 location of the occulted star with its ICRF position from the Hipparcos catalogue.[14]

To assist in determining the planet and satellite orbits we added the following data sets to the Voyager data:

- satellite astrometry derived from telescopic observations made at several astronomical observatories over the time period 1847 to 2007. The sources of the pre-1990 observations are provided in Ref. 4. Post-1990 observations are: charged couple device (CCD) observations from the Laboratório Nacional de Astrofísica (LNA) in Brazil (1991–2002), CCD observations from McDonald Obs. (1993–1994), photographic and CCD observations from the USNO at Flagstaff (1995–2007), meridian circle obsevations from Bordeaux Obs. (1999–2005), CCD observations from Table Mtn. Obs. (1999–2007), and CCD observations (1990–2007) of Nereid that were reported to the Minor Planet Center at the Smithsonian Astrophysical Obs.[15] by several observers.
- planet astrometry over the time period 1904–2006. These included visual observations of Neptune relative to a nearby star made at Yerkes Obs. (1904–1922), photographic and CCD observations from Nikolaev Obs. (1962–1998), and observations made concurrent with some of the satellite astrometry (USNO at Flagstaff, Bordeaux Obs., and Table Mtn.).

- planet transit observations over the time period 1934 to 1996; these are the same observations used in the development of the JPL planetary ephemeris DE421.[16]
- planet occultation measurements in the form of the occultation times. These are stellar occultations of the planet seen from Earthbased observatories during the period 1968 to 1989. See Refs. 17–23 for a discussion of the occultations. For the stellar occultations, as with the Voyager UVS stellar occultation, we replaced the original B1950/FK4 locations of the occulted stars with ICRF positions from either the UCAC2 star catalogue or the Hipparcos catalogue.

II.B. Dynamical Model

Our dynamical model contained both gravitational and non-gravitational forces; the former affect the motion of the spacecraft, planet, and satellites, whereas the latter affect only the spacecraft. Sources of the gravitational forces were the Sun, the solar system planets, and the Neptunian satellites. The gravity field of the planet was represented by the standard spherical harmonic expansion of its gravitational potential; we retained only the second and fourth zonal harmonics. We represented the pole of Neptune by a vector which precesses about the angular momentum vector of the Neptunian system; this polar motion is driven by the torque due to the gravitational attraction of Triton on the planet's equatorial bulge. Model details may be found in Ref. 4.

JPL planetary ephemeris DE421[16] provided the positions and masses of the Sun and planets with the exception of Neptune; the ephemeris of Neptune was a differential correction to DE421 based on our data fit.

Solar radiation pressure effects on the spacecraft were modelled with the formulation of Georgevic.[24] The values of the parameters in the models were determined during the Earth-Jupiter cruise period: we retained those values.

The Voyager spacecraft was three-axis stabilized. The Z axis was the axis of symmetry of the spacecraft bus and the X and Y axes were the pitch and yaw axes, respectively; the centerline of the high gain antenna was aligned with the Z axis and was normally pointed toward the Earth. Attitude was changed and maintained by groups of thrusters which were unbalanced, i.e., they did not fire in pairs separated from the center of mass on opposite moment arms. Consequently, there was a net translational velocity imparted to the spacecraft each time a thruster was fired. In addition, due to a design flaw, the exhaust plumes from the pitch thrusters struck the spacecraft adding to the translational velocity when they were fired. We included impulses along the spacecraft coordinate axes at the times of a number of the larger attitude changes to account for the translations. The remaining attitude control pulses were modelled as the sum of constant and stochastic accelerations along the spacecraft axes. This model also absorbed the effects of non-isotropic thermal radiation from the RTGs (Pu^{238} radioisotope thermoelectric generators which provided electrical power) and solar pressure mis-modelling. The non-gravitational accelerations were a major source of Voyager navigation error; Ref. 25 contains an excellent discussion of them.

During the time frame of our analysis the spacecraft made three trajectory correction maneuvers (TCM); we modelled the two smallest ones as impulses and the largest, TCM18, with the finite burn (rocket equation) model. The velocity changes imparted by the spacecraft attitude control and trajectory correction maneuvers appear in Table 1. Except for TCM18 all changes are referred to the spacecraft axes. For TCM18 the table contains the ICRF coordinates of the velocity change accumulated during the maneuver. The acronyms designating the events are:

- ASCAL – high gain antenna signal pattern and Sun sensor alignment check
- CDT – capability demonstration test
- DTR – digital tape recorder
- MAGROLL – spacecraft roll for magnetometer
- NIMC – nodding image motion compensation
- ORT – operational readiness test
- RSS – radio science

- VPHASE – imaging of Neptune's limb
- VTCOLOR – highest resolution color imaging of Triton
- VTERM – highest resolution imaging of Triton

II.C. Method of Solution

We determined the orbits of the spacecraft, the planet, and the satellites by adjusting parameters in the dynamical and observational models to obtain a weighted least-squares fit to the observational data. The adjustable parameters are summarized in Table 2.

Our processing procedure was essentially the same as that employed in our Jupiter, Saturn, and Uranus ICRF reconstructions and had none of the limitations which affected the original Neptune work. For example, we no longer were limited in the number of parameters we could estimate and, as a consequence, could employ a longer data arc and simultaneously determine all relevant parameters. In addition, our current software permitted a more sophisticated treatment of stochastic parameters and allowed us to include tracking pass dependent biases in the range data and biases in the three-way Doppler.

We processed the observations with a batch-sequential, square-root information filter, treating the stochastic non-gravitational accelerations, camera pointing angles, range biases, and three-way Doppler biases as white noise. The four separate range biases applied to the two-way range and three-way range from each of the three transmitter-receiver pairs. Analogously, there was a separate three-way Doppler bias for each transmitter-receiver pair. The accelerations were batched at 1 day intervals with additional batches at the times of the spacecraft attitude changes. The pointing angles were batched by picture, and the range biases were batched by tracking pass. The three-way Doppler biases were designed to account for calibration errors; their batches were aligned with the roughly 14 day time spans of the calibration sets.

We estimated two disjoint constant accelerations along the Z-axis, one for the low activity time period prior to the start of the Observatory phase and one for the high activity period begining with the Observatory phase and extending to the end of our data arc. The constant accelerations normal to the Z-axis applied to the entire time span of the analysis.

The parameters that we adjusted in the Neptune pole model were: the right ascension and declination of Neptunian system angular momentum vector, the angle between the Neptune pole and the angular momentum vector, the angle between the Triton orbit normal and the angular momentum vector, the pole precession angle at epoch, and the pole precession rate.

For each of the three one-way Doppler passes we estimated a spacecraft transponder oscillator frequency bias, and for the longer of the passes we estimated a frequency drift as well. In addition to the pass by pass ranges biases, we determined a global range bias for each DSN complex. We also found a scale factor adjustment for the solar corona model which accounted for range delay due to solar plasma. In order to properly process the ΔDOR data we had to adjust the quasar locations, and when fitting the occultation observations, we had to correct the radii of Neptune and Triton and the star locations. The refraction corrections noted in Table 2 applied to two sets of the Neptune astrometry.

In our estimation process we included *a priori* information for the spacecraft maneuvers and non-gravitational accelerations; it was essentially the same as that used in the previous reconstruction. We constrained the corrections to the occultation star positions by the quoted uncertainties in their catalogue positions; an analogous constraint was placed on the quasar position corrections based on the uncertainties in their ICRF locations. When processing the Triton occultations we used the Triton radius of 1352.6 km determined from Voyager imaging[26] and limited the radius correction by the 2.4 km uncertainty associated with that value.

With multiple data types data weights balance the information provided by each type as well as represent the accuracy of the type. Assigning the weights is as much an art as a science. Our selections were guided by knowledge of the potential accuracy of the type coupled with an examination of the data residuals.

We set separate Doppler data weights for each DSN pass to correspond to an accuracy consistent with the root-mean-square (rms) of the residuals for that pass. We also applied a scale factor to the rms to account

for the fact that the Doppler noise is not a white-noise process.[27] The scale factor was $0.468\,(86400/\tau)^{1/3}$ where τ is the sample interval in seconds (for a 5 minute sample interval the factor is 3.09). The scale factor preferentially weighted the Doppler at the diurnal frequency (86400 s); it yielded a conservative weight which was too conservative for the encounter data. For the encounter passes on 25 August we adopted the Doppler whitening algorithm[28] which was developed for Cassini planetary gravity analysis.

We weighted the range data on a pass-by-pass basis with weights derived from the rms of the data residuals scaled by the square root of the number of points in the pass. The scaling suppressed range rate information inferred from the change in the range during the pass; the Doppler data then became the primary source of range rate information. We also imposed limits on the weights by requiring that the scaled rms of two-way range passes be greater than 25 m and three-way passes be greater than 50 m. The stochastic range biases accounted for range calibration errors and systematically deweighted the range data. The biases had 100 m *a priori* uncertainties.

We set the ΔDOR data weights to represent a timing delay accuracy of 1 nanosecond which translates into a position error of roughly 150 km at Neptune. This weight is a factor of 3 tighter than that used in mission operations, but we found the tighter weight necessary to balance the ΔDOR data relative to the Doppler and range.

The accuracy assumed for most of the imaging data was 0.25 pixels for the stars, 0.5 pixels for Triton and Nereid, and 1.0 pixels for Proteus. The post-encounter satellite images were systematically deweighted up to 2.0 pixels uncertainty because of centerfinding problems introduced by their high phase angles. These accuracies are about a factor of two better than those assumed previously; we found that the accuracies used in mission operations were clearly pessimistic.

The occultation observables are the recorded occultation times; we adopted the suggested accuracies provided by the observers.

The planet and satellite astrometric and transit data were grouped according to data type, observatory, and the observing period during which they were acquired. The accuracy of each group was taken to be equal to the rms of residuals of the group. In addition we dewighted the entire Earthbased data set by a factor of 3 relative to the spacecraft data set. We found that this relative weighting produced a better fit of the planet and satellite orbits to the combined Earthbased and spacecraft data.

III. Results

The Voyager trajectory at Neptune was designed to support two major science objectives: a Neptune occultation of the spacecraft which enabled the radio signal to probe the planet's atmosphere, and dual radio and stellar occultation at Triton to collect data on that satellite's atmosphere. To achieve the objectives, the spacecraft was targeted to an arrival time at Neptune and at pair of B-plane coordinates at Triton. Table 3 contains the B-plane coordinates and the time of closest approach with estimated actual uncertainties from the previous reconstruction and ours. Because that earlier work was carried out in the B1950/FK4 system, we give our results in both that system and the ICRF. The agreement between the results is excellent considering the differing reference frames, models, and estimation procedures. Much of the difference in the Triton B-plane is due to a 5 km difference between the positions from the previous Triton orbit and our current one. Figure 1 displays the differences between our reconstructed Voyager trajectory and the previous one in the directions radial from Neptune, along the trajectory, and normal to the trajectory plane. The trajectories differ by tens of kilometers at times away from Neptune closest approach, but converge at the Neptune encounter.

The estimated velocity changes imparted by the spacecraft attitude control and trajectory correction maneuvers appear in Table 1. There was not sufficient data coverage to determine all of the impulsive manuvers. Those not estimated are so designated in the table; we used their predicted values in our trajectory propagation.

The values of the constant non-gravitational accelerations along the X and Y spacecraft axes were 0.284×10^{-12} km s^{-2} and 3.730×10^{-12} km s^{-2}; along the Z axis the acceleration was -0.142×10^{-12} km s^{-2} before

1 June and -0.829×10^{-12} km s^{-2} after 1 June. The largest acceleration is along the Y axis, a consequence of the thruster impingement during attitude control burns mentioned earlier in this paper. Figure 2 shows the stochastic acceleration along the Z axis; the accelerations along the other axes are more than an order of magnitude smaller. The stochastic acceleration is near the expected level of 2×10^{-12} km s^{-2}. Note the increase in the level after the 1 June as a consequence of approach and encounter activities.

Our estimated gravity field and pole model parameter values and those obtained previously[4] appear in Table 4 along with their adopted uncertainties. The reference radius for the gravity harmonics, J_2 and J_4, is 25225 km. The ICRF right ascension, α_p, and declination, δ_p, of the Neptune pole are computed from the pole model which depends on the parameters:

- α_r – the right ascension of the Neptunian system angular momentum vector
- δ_r – the declination of the Neptunian system angular momentum vector
- ϵ – the angle between the Neptune pole and the Neptunian system angular momentum vector
- I – the angle between the normal to Triton's orbital plane and the Neptunian system angular momentum vector
- Ω – the pole precession angle on 25 August 1989
- $\dot{\Omega}$ – the pole precession rate

Our values for the masses and harmonics agree with those obtained earlier, and our pole orientation at the time of the Neptune encounter also matches the previous pole within the uncertainties although the pole models were slightly different.

We estimated corrections to the Neptune ephemeris of the order of 100 km in the in-orbit direction, 50 km in the radial direction, and 350 km in the out-of-plane direction during the Voyager encounter period. The corrections are consistent with the uncertainty associated with DE421. Our Triton orbit differed from that described in Ref. 4 by about 100 km, primarily in the direction normal to the orbital plane. We found an increase in Nereid's orbital period of about 1.2 minutes and decrease in eccentricity of about 0.0005; the former translates into a downtrack change of about 80 km/yr, and the latter translates into periodic radial differences of about 2700 km and periodic downtrack differences of about 5500 km. Like Triton, the orbit of Proteus changed primarily in the normal direction, differing from that described in Ref. 29 by about 300 km.

Figures 3 and 4 display the stochastic three-way Doppler and range biases, respectively. The Doppler biases are roughly an order of magnitude below the calibrations suggesting that little can be done to improve the calibrations. The range biases have an rms of about 50 m with some biases approaching nearly 250 m.

The spacecraft data residuals shown in Figures 5–15 give an idea of the data spans, noise levels, and quality of the data fit. Our fit is as good if not slightly better than that done for the earlier navigation reconstruction because of the improvements in the dynamical and observational modelling. The Doppler noise during the encounter period on 25 August is higher because the data there were compressed to a 5 second sample interval. The compression interval away from the encounter varied between 1 minute and 20 minutes depending upon the spacecraft activity at the time; higher activity called for shorter intervals in order to more accurately measure the spacecraft motion. The optical residuals are well within the observational uncertainties. They are a bit noisier than those shown in the previous reconstruction because the tighter weights on the star observations more tightly constrained the camera pointing. The degradation of the fit to the post-encounter Triton images is attributed to centerfinding errors.

Table 5 compares the Triton occultation residuals from the previous reconstruction and the current one. Clearly, the radio occultations are in good agreement, but the UVS occultations exhibit minor disagreement. There is a large uncertainty associated with the UVS ingress time, and our residual is well within that uncertainty. However, our UVS egress time residual slightly exceeds the measurement uncertainty. There has always been somewhat of a conflict between the radio and UVS occultation measurements and some question as to the true accuracy of the UVS timing. Because we can easily fit the radio occultation along with the rest of our data and but cannot reduce the UVS egress residual to below its weight, we conjecture that the egress time uncertainty is optimistic.

IV. Conclusion

In this paper we have reported a new reconstruction of the Voyager Neptune encounter trajectory. The reconstruction was done as part of an investigation of the Neptunian system gravity field and the orbits of Neptune and its satellites. The new trajectory was needed in order to properly process the Voyager tracking and optical navigation data for that investigation. Because of improvements in our models and data processing procedures and our use of the modern ICRF reference frame, we believe the new trajectory to be the most accurate description produced thus far for the spacecraft motion through the Neptunian system. The work completes the sequence of Voyager reconstructions in the ICRF system.

Acknowledgments

We would like to thank Bill Owen for converting the Voyager optical data to the ICRF system. The research described in this paper was performed at the Jet Propulsion Laboratory, California Institute of Technology, under contract with the National Aeronautics and Space Administration. Copyright 2008 California Institute of Technology. Government sponsorship acknowledged.

References

[1]Lewis, G. D., Taylor, A. H., Jacobson, R. A., Roth, D. C., Riedel, J. E., Synnott, S. P., and Ryne, M., "Voyager 2 Orbit Determination at Neptune," AIAA Paper 90-2879 AIAA/AAS Astrodynamics Conference, Portland, OR, 1990, American Institute of Aeronautics and Astronautics, Reston, VA.

[2]Roth, D. C., Taylor, A. H., Jacobson, R. A., and Lewis, G. D., "Performance of Three-way Data Types During Voyager's Encounter with Neptune," AIAA Paper 90-2878 AIAA/AAS Astrodynamics Conference, Portland, OR, 1990, American Institute of Aeronautics and Astronautics, Reston, VA.

[3]Riedel, J. E., Owen, W. M., Stuve, J. A., Synnott, S. P., and Vaughan, R. M., "Optical Navigation during the Voyager Neptune Encounter," AIAA Paper 90-2877 AIAA/AAS Astrodynamics Conference, Portland, OR, 1990, American Institute of Aeronautics and Astronautics, Reston, VA.

[4]Jacobson, R. A., Riedel, J. E., and Taylor, A. H., "The orbits of Triton and Nereid from spacecraft and Earthbased observations," *A&A*, Vol. 247, 1991, pp. 565–575.

[5]Jacobson, R. A., "Pioneer and Voyager Jupiter Encounter Orbit Reconstruction in the ICRF System," AAS Paper 02-157 AAS/AIAA Space Flight Mechanics Meeting, San Antonio, TX, 2002, American Astronautical Society, Springfield, VA.

[6]Jacobson, R. A., "Reconstruction of the Voyager Saturn Encounter Orbits in the ICRF System," AAS Paper 03-198, 13th AAS/AIAA Space Flight Mechanics Meeting, Ponce, PR, 2003, American Astronautical Society, Springfield, VA.

[7]Jacobson, R. A. and Rush, B., "Reconstruction of the Voyager Uranus Encounter in the ICRF System," AAS Paper 07-319, 2007 AAS/AIAA Astrodynamics Specialist Conference, Mackinac Island, MI, 2007, American Astronautical Society, Springfield, VA.

[8]Ma, C., Arias, E. F., Eubanks, T. M., Fey, A. L., Gontier, A. M., Jacobs, C. S., Sovers, O., J., Archinal, B., A., and Charlot, P., "The International Celestial Reference Frame as Realized by Very Long Baseline Interferometry," *AJ*, Vol. 116, 1998, pp. 516.

[9]Jacobson, R. A., "The Orbits of the Neptunian Satellites and the Orientation of the Pole of Neptune," *BAAS*, Vol. 40, No. 2, 2008, pp. 296, presented at the 39th annual meeting of the American Astronomical Society Division on Dynamical Astronomy, Boulder, CO.

[10]Connally, M. J., "DSN Telecommunications Link Design Handbook," Tech. Rep. 810-005, Rev. E, Jet Propulsion Laboratory, 2006, Module 107: Radio Source Catalog.

[11]Border, J. S., Donivan, F. F., Finley, S. G., Hildebrand, C. E., Moultrie, B., and Skjerve, L. J., "Determining Spacecraft Angular Position with Delta VLBI: The Voyager Demonstration," AIAA Paper No. 82-1471 AIAA/AAS Astrodynamics Conference, San Deigo, CA, 1982, American Institute of Aeronautics and Astronautics, Reston, VA.

[12]Taylor, A. H., Campbell, J. K., Jacobson, R. A., Moultrie, B., Nichols, Jr., R. A., and Riedel, J. E., "Performance of Differenced Range Data Types in Voyager Navigation," AIAA Paper 82-1473 AIAA/AAS Astrodynamics Conference, San Diego, CA., 1982, American Institute of Aeronautics and Astronautics, Reston, VA.

[13]Zacharias, N., Urban, S. E., Zacharias, M. I., Wycoff, G. L., Hall, D. M., Monet, D. G., and Rafferty, T. J., "The Second US Naval Observatory CCD Astrograph Catalog (UCAC2)," *AJ*, Vol. 127, 2004, pp. 3043–3059.

[14]ESA, "The Hipparcos and Tycho Catalogues," ESA-SP 1200, European Space Agency, 1997.

[15]The Minor Planet Center, Smithsonian Astrophysical Observatory, Cambridge, MA 02123, http://cfa-www.harvard.edu/iau/mpc.html.

[16]Folkner, W. M., Williams, J. G., and Boggs, D. H., "The Planetary and Lunar Ephemeris DE421," Interoffice Memo. 343R-08-003 (internal document), Jet Propulsion Laboratory, Pasadena, CA, 2008, Pasadena:JPL.

[17]Kovalevsky, J. and Link, F., "Diametre, Flattening and Optical Properties of the Upper Atmosphere of Neptune as Derived from the Occultation of BD-17°4388," *A&A*, Vol. 2, 1969, pp. 398–412.

[18]French, R. G., Elias, J. H., Mink, D. J., and Elliot, J. L., "The Structure of Neptune's Upper Atmosphere: The Stellar Occultation of 24 May 1981," *Icarus*, Vol. 55, 1983, pp. 332–336.

[19]French, R. G., Melroy, P. A., Baron, R. L., Dunham, E. W., Meech, K. J., Mink, D. J., Elliot, J. L., Allen, D. A., Ashely, M. C. B., Freeman, K. C., Erickson, E. F., Goguen, J., and Hammel, H. B., "The 1983 June 15 Occultation by Neptune. II. The Oblateness of Neptune," *AJ*, Vol. 90, 1985, pp. 2624–2638.

[20]Hubbard, W. B., Frecker, J. E., Gehrels, J. A., Gehrels, T., Hunten, D. M., Lebofsky, L. A., Smith, B. A., Tholen, D. J., Vilas, F., Zellner, B., Avey, H. P., Mottram, K., Murphy, T., Varnes, B., Carter, B., Neilsen, A., Page, A. A., Fu, H. H., Wu, H. H., Kennedy, H. D., Waterworth, M. D., and Reitsema, H. J., "Results from Observations of the 15 June 1983 Occultation by the Neptune System," *AJ*, Vol. 90, 1985, pp. 655–667.

[21]Covault, C. E., Glass, I. S., French, R. G., and Elliot, J. L., "The 7 and 25 June 1985 Neptune Occultations: Constraints of the Putative Neptune "Arc"," *Icarus*, Vol. 67, 1986, pp. 126–133.

[22]Nicholson, P. D., Cooke, M. L., and Pelton, E., "An Absolute Radius Scale for Saturn's Rings," *AJ*, Vol. 100, 1990, pp. 1339–1362.

[23]Sicardy, B., Roques, F., and Brahic, A., "Neptune's Rings, 1983–1989: Ground-Based Stellar Occultation Observations," *Icarus*, Vol. 89, 1991, pp. 220–243.

[24]Georgevic, R. M., "Mathematical Model of the Solar Radiation Force and Torques Acting on the Components of a Spacecraft," JPL TM 33-494 (internal document), Jet Propulsion Laboratory, Pasadena, CA, 1971.

[25]Campbell, J. K., Synnott, S. P., Riedel, J. E., Mandell, S., Morabito, L. A., and Rinker, G. C., "Voyager 1 and Voyager 2 Jupiter Encounter Orbit Determination," AIAA Paper No. 80-0241 AIAA 18th Aerospace Sciences Meeting, Pasadena, California, 1980, American Institute of Aeronautics and Astronautics, Reston, VA.

[26]Davies, M. E., Rogers, P. G., and Colvin, T. R., "A Control Network of Triton," *JGR*, Vol. 96, No. E1, 1991, pp. 15,675–15,681.

[27]Folkner, W. M., "Effect of uncalibrated particles on Doppler tracking," IOM 335.1-94-005 (internal document), Jet Propulsion Laboratory, Pasadena, CA, 1994.

[28]Mackenzie, R. A. and Folkner, W. M., "Whitening Doppler data for Planetary Gravity Field Determination," IOM 343J-06-034 (internal document), Jet Propulsion Laboratory, Pasadena, CA, 2006.

[29]Jacobson, R. A. and Owen, Jr., W. M., "The orbits of the inner Neptunian satellites from Voyager, Earth-based, and Hubble Space Telescope observations," *AJ*, Vol. 128, 2004, pp. 1412–1417.

Table 1. Maneuvers (mm sec^{-1})

Time(TDB)		$\Delta\dot{X}$	$\Delta\dot{Y}$	$\Delta\dot{Z}$	Event
17-Nov-1988	23:12:00	0.178	1.635	−0.542	RSS ORT
13-Dec-1988	05:25:00	0.300	0.800	0.000	DTR test†
24-JAN-1989	00:05:00	0.500	1.600	0.000	DTR test†
2-Feb-1989	20:02:22	3.037	14.215	−8.138	Mini cruise maneuver
24-Feb-1989	13:08:00	−0.456	2.322	−0.734	RSS CDT & DTR test
27-Feb-1989	19:00:00	0.344	10.152	−4.152	NIMC & DTR test
20-Mar-1989	12:00:00	0.300	0.800	0.000	DTR test†
22-Mar-1989	10:03:29	0.000	0.200	0.000	ASCAL†
23-Mar-1989	15:08:00	0.000	0.700	−0.100	RSS ORT†
3-Apr-1989	12:00:00	0.300	0.800	0.000	DTR test†
20-Apr-1989	16:19:46	91.925	−339.117	−10.428	TCM17
26-Apr-1989	21:44:20	32.383	10.477	−0.738	Roll to Alkaid
27-Apr-1989	12:52:00	−0.381	0.701	−0.297	RSS ORT
4-May-1989	14:45:57	−1.594	1.764	−0.012	Target maneuver
8-May-1989	12:32:52	34.538	−1.933	−4.917	unknown calibration
16-May-1989	15:16:22	−1.440	−8.477	−5.421	MAGROLL
25-May-1989	16:29:39	4.896	4.103	−6.758	Roll turns
12-Jun-1989	14:04:37	0.028	−0.063	−0.239	ASCAL
15-Jun-1989	17:26:59	−2.983	13.927	−7.933	Mini cruise maneuver
26-Jun-1989	13:01:11	−0.875	−2.374	−1.749	Roll to Spica then to Achernar
22-Jul-1989	00:00:34	23.029	15.277	1.975	Roll to Spica
22-Jul-1989	05:49:11	24.643	−16.035	−3.845	Roll to Achernar
1-Aug-1989	12:55:18	−335.093	−850.755	−161.348	TCM18‡
1-Aug-1989	14:55:30	0.185	1.868	−0.920	TCM18 turns†
7-Aug-1989	06:44:56	−2.524	2.690	−1.185	ASCAL
15-Aug-1989	16:23:03	0.499	8.382	−0.834	Roll to Canopus
21-Aug-1989	12:48:06	−477.544	−8.441	−12.920	TCM20
24-Aug-1989	21:30:43	−0.011	0.272	−0.015	NIMC #1-6
25-Aug-1989	00:49:07	−0.105	0.076	0.034	NIMC #7
25-Aug-1989	01:06:43	−0.001	0.076	−0.039	NIMC #8
25-Aug-1989	01:30:43	0.002	0.077	−0.120	NIMC #9
25-Aug-1989	01:34:31	0.002	0.077	−0.044	NIMC #10

†not estimated ‡ICRF coordinates

Table 1. Maneuvers (mm sec^{-1}) – Continued

Time(TDB)	$\Delta\dot{X}$	$\Delta\dot{Y}$	$\Delta\dot{Z}$	Event
25-Aug-1989 03:04:19	−15.524	25.468	−0.762	Roll to +61 deg
25-Aug-1989 03:17:46	0.000	0.800	−0.100	ASCAL†
25-Aug-1989 04:13:35	−0.500	1.100	0.400	Limbtrack, part 1†
25-Aug-1989 04:25:47	0.500	0.900	0.500	Limbtrack, part 2†
25-Aug-1989 04:37:30	−0.028	−0.812	−1.947	Limbtrack, part 3
25-Aug-1989 04:51:47	−0.644	0.620	0.292	Limbtrack, part 4†
25-Aug-1989 05:27:22	0.988	2.408	−0.603	ASCAL
25-Aug-1989 05:38:34	0.948	2.146	0.191	VPHASE
25-Aug-1989 05:55:17	−54.590	10.686	−1.367	Roll to Alkaid
25-Aug-1989 06:27:20	3.118	3.474	−1.787	VTCOLOR
25-Aug-1989 07:17:07	−0.049	−0.728	−0.240	NIMC #11-16
25-Aug-1989 07:45:55	−0.019	0.055	−0.160	NIMC #17-22
25-Aug-1989 08:14:43	0.038	1.487	−0.156	NIMC #23-28
25-Aug-1989 08:56:08	0.100	0.600	0.200	VTERM†
25-Aug-1989 08:59:01	−2.516	11.789	2.296	Pitch +21 deg
25-Aug-1989 10:08:08	−53.097	16.479	−1.325	Roll to Canopus
28-Aug-1989 09:36:05	17.268	15.312	−0.734	Roll to Spica
28-Aug-1989 21:00:06	−16.496	17.494	−0.789	Roll to Canopus
5-Sep-1989 09:12:53	16.503	17.710	−0.704	Roll to Spica
7-Sep-1989 19:38:30	−15.492	16.402	−0.871	Roll to Canopus
8-Sep-1989 23:02:02	0.000	0.200	0.000	ASCAL†
13-Sep-1989 06:40:42	−0.682	5.446	−9.425	Mini cruise maneuver
25-Sep-1989 14:20:23	−0.995	1.792	0.540	Target maneuver
28-Sep-1989 21:13:43	15.300	15.800	−0.200	Roll to Spica†
29-Sep-1989 06:02:31	−15.793	16.405	−0.894	Roll to Canopus

†not estimated

Table 2. Estimated Parameters

Spacecraft		Ephemeris	
Position and velocity	(6)	Neptune orbital elements	(6)
Constant accelerations	(4)	Triton position and velocity	(6)
Impulsive velocity changes	(126)	Nereid position and velocity	(6)
Finite burn thrust and direction	(3)	Proteus position and velocity	(6)
Dynamic		Stochastic	
Neptunian system GM	(1)	Spacecraft accelerations	(3)
Neptune gravitational harmonics	(2)	Camera pointing angles	(3)
Neptune pole model parameters	(6)	Range biases	(4)
Triton GM	(1)	Three-way Doppler biases	(3)
Non-Dynamic			
One-way Doppler biases and drift	(4)		
Range biases	(3)		
Quasar locations	(4)		
Solar corona model scale factor	(1)		
Neptune equatorial and polar radii	(2)		
Triton radius	(1)		
Star locations	(16)		
Refraction corrections	(2)		

Table 3. Neptune Encounter Geometry and Times

Case	B·R (km)	B·T (km)	Time of Closest Approach
		Neptune B-Plane	
RECON2[†]	-42983.8 ± 2.0	-20954.8 ± 2.0	25 Aug 1989 03:56:36.30 ± 0.10
B1950	-42983.8 ± 0.5	-20954.7 ± 0.5	25 Aug 1989 03:56:36.27 ± 0.05
ICRF	-42985.0 ± 0.5	-20952.2 ± 0.5	25 Aug 1989 03:56:36.27 ± 0.05
		Triton B-Plane	
RECON2[†]	-39480.6 ± 12.7	4906.9 ± 13.8	25 Aug 1989 09:11:02.8 ± 0.6
B1950	-39478.0 ± 9.7	4900.6 ± 10.5	25 Aug 1989 09:11:03.0 ± 0.4
ICRF	-39477.9 ± 9.7	4903.1 ± 10.5	25 Aug 1989 09:11:03.0 ± 0.4

[†]from Ref. (1)

Table 4. Dynamic Parameters

Parameter	Previous†	Current
GM ($km^3 s^{-2}$)		
System	6836534.9 ± 15.0	6836527.3 ± 10.0
Triton	1427.9 ± 3.5	1427.6 ± 1.8
J_2 ($\times 10^6$)	3410.5 ± 9.0	3408.5 ± 4.6
J_4 ($\times 10^6$)	-34.7 ± 10.0	-33.5 ± 2.9
α_p (deg)	299.27 ± 0.15‡	299.36 ± 0.14‡
δ_p (deg)	42.95 ± 0.05‡	42.89 ± 0.02‡
α_r (deg)	299.36 ± 0.15	299.46 ± 0.14
δ_r (deg)	43.45 ± 0.05	43.39 ± 0.02
ϵ (deg)	0.506	0.442 ± 0.003
I (deg)	156.834	156.894 ± 0.001
Ω (deg)	352.43‡	352.18 ± 0.33‡
$\dot{\Omega}$ (deg century^{-1})	52.32	52.42 ± 0.08

†from Ref. (4) ‡at epoch 25 August 1989

Table 5. Triton Occultation Residuals

Occultation	Ingress (s)			Egress (s)		
	Weight	RECON2	Current	Weight	RECON2	Current
Radio Science	0.02	−0.013	−0.011	0.02	−0.001	0.002
UVS (star)	3.00	0.320	0.990	0.32	−0.211	−0.383

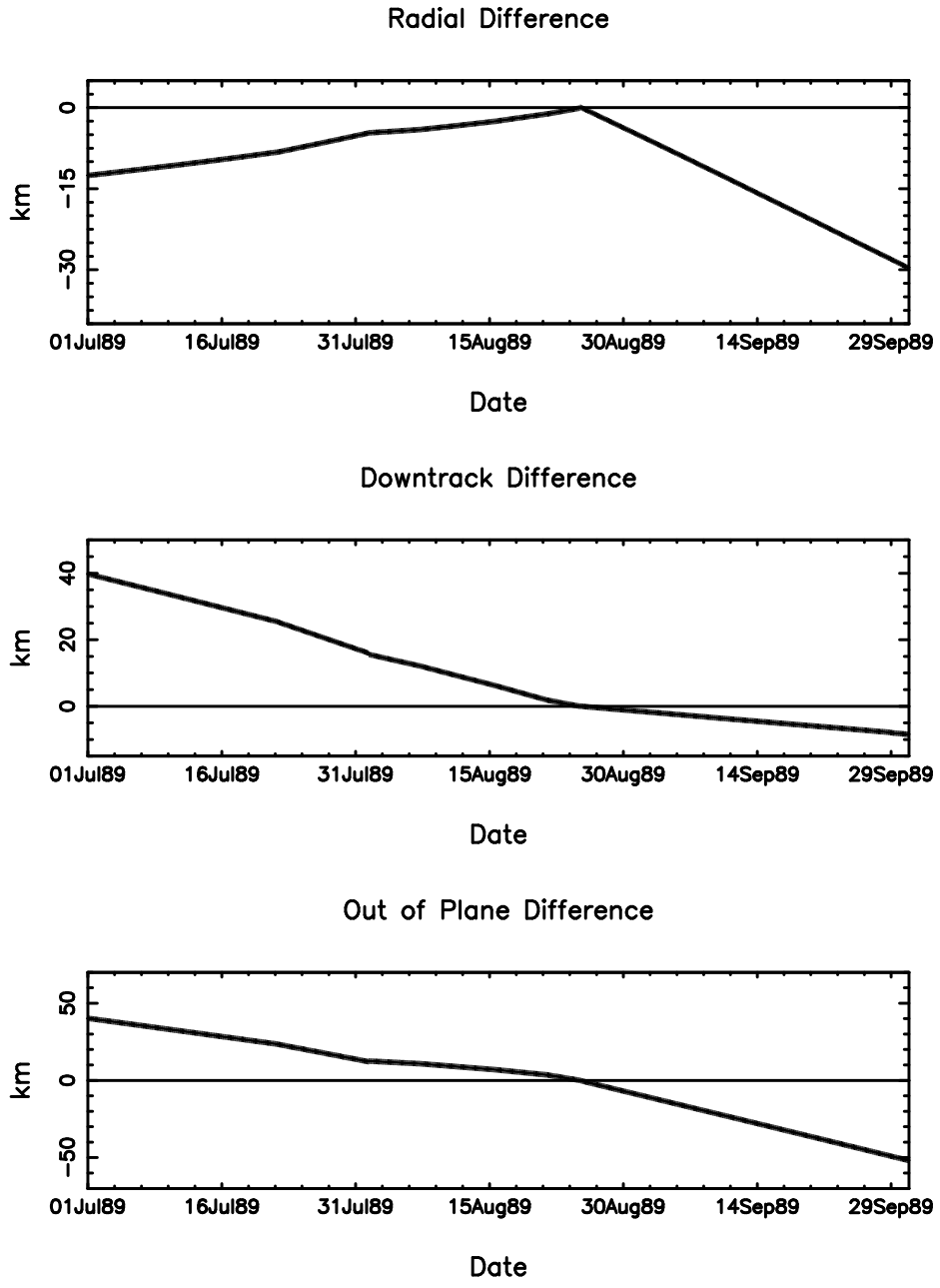

Figure 1. Comparison of the Previous Voyager Trajectory and the Current Reconstruction

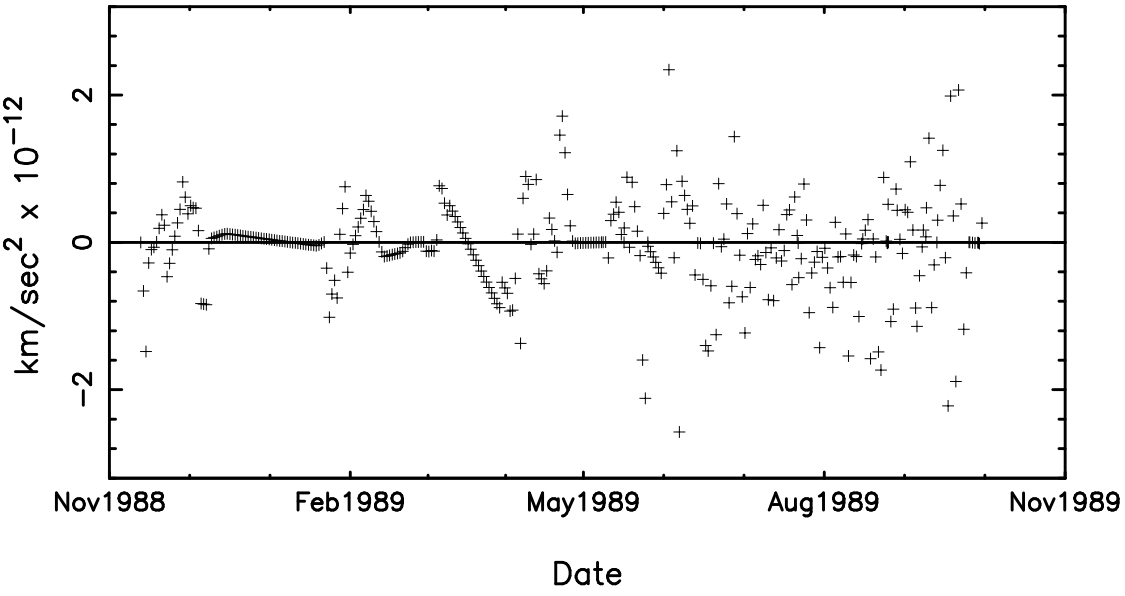

Figure 2. Z Stochastic Acceleration

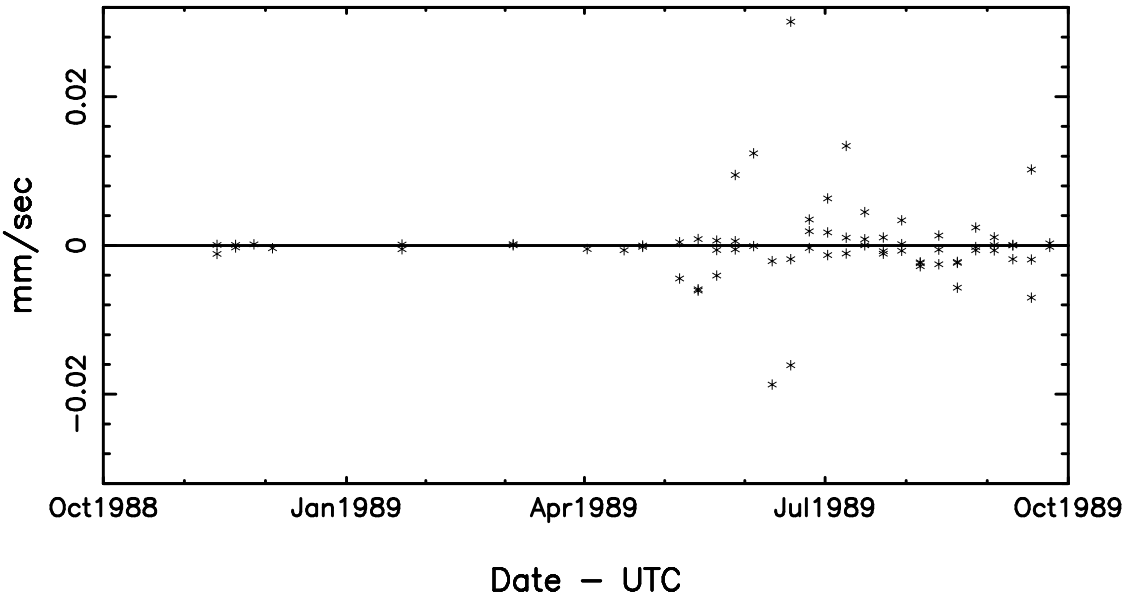

Figure 3. Three-way Doppler Biases

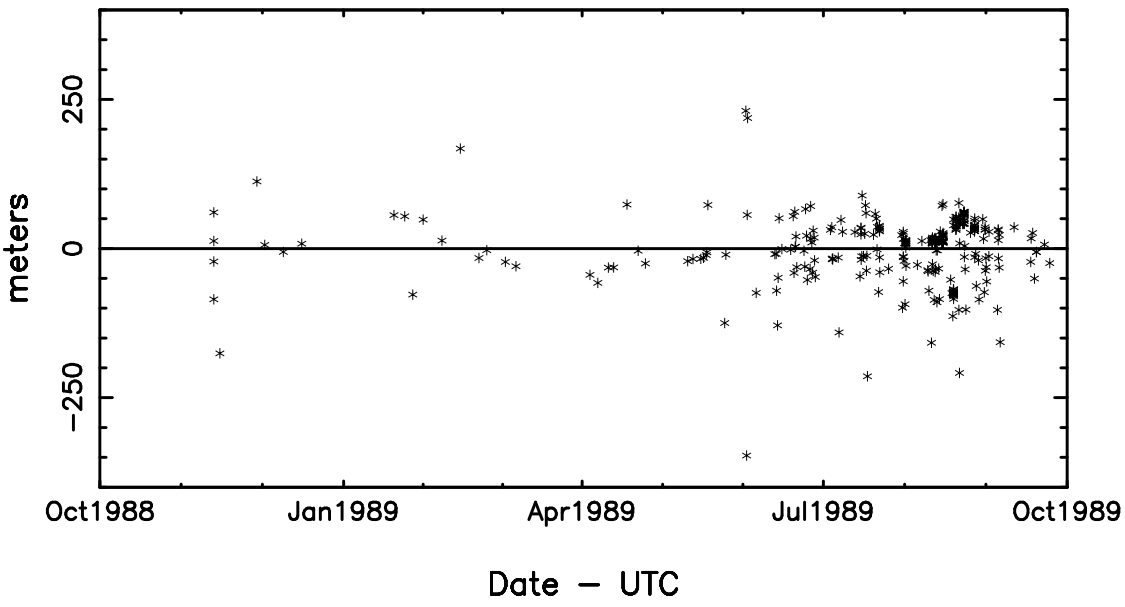

Figure 4. Range Biases

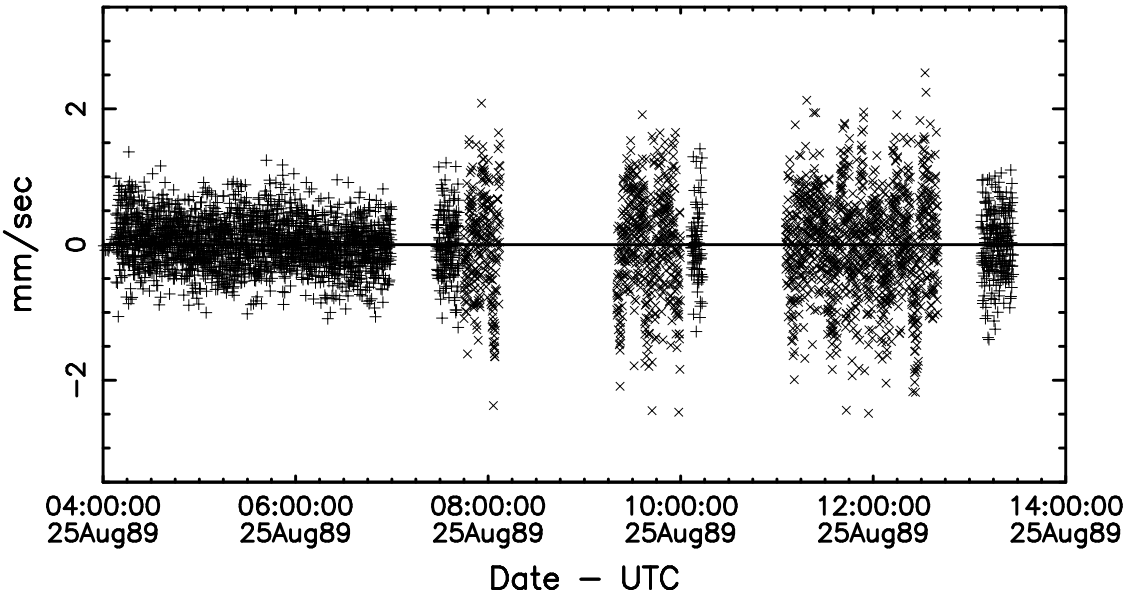

Figure 5. Encounter Doppler Residuals

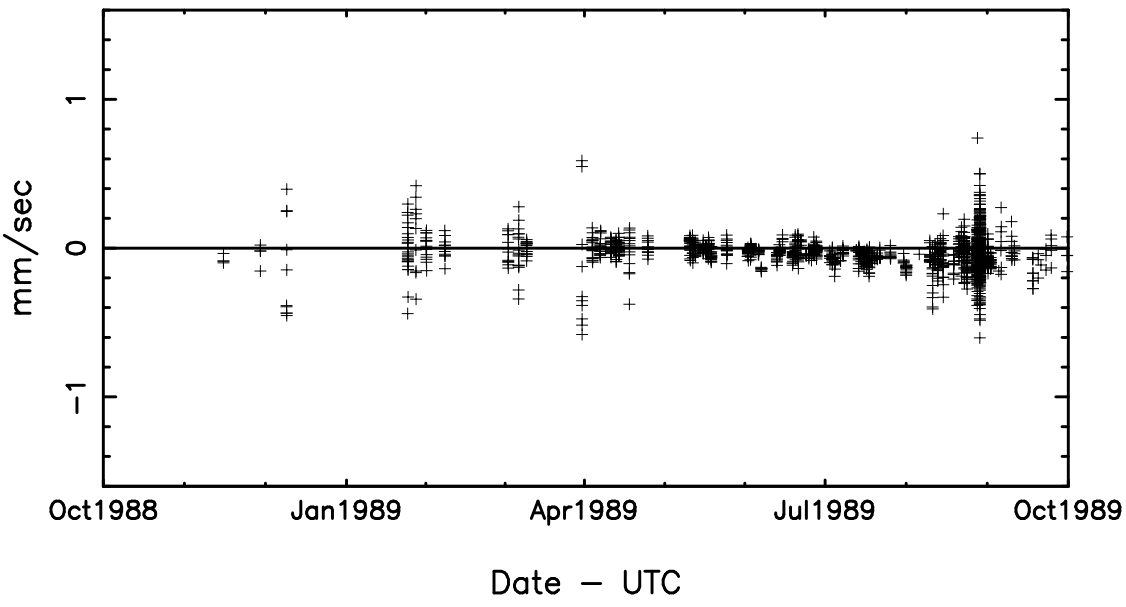

Figure 6. Two-Way Doppler Residuals

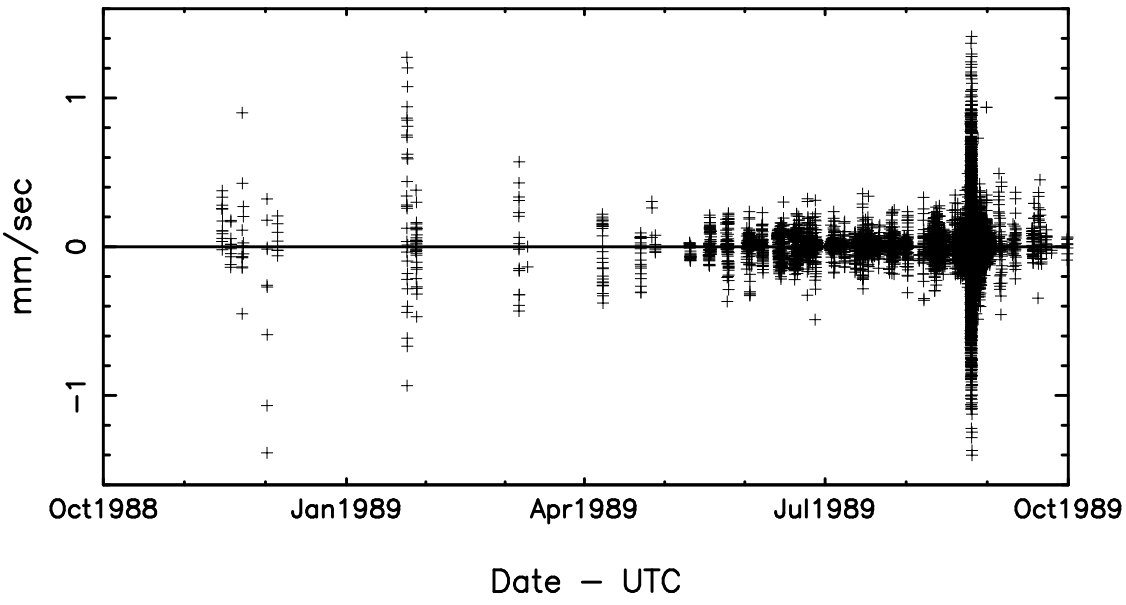

Figure 7. Three-Way Doppler Residuals

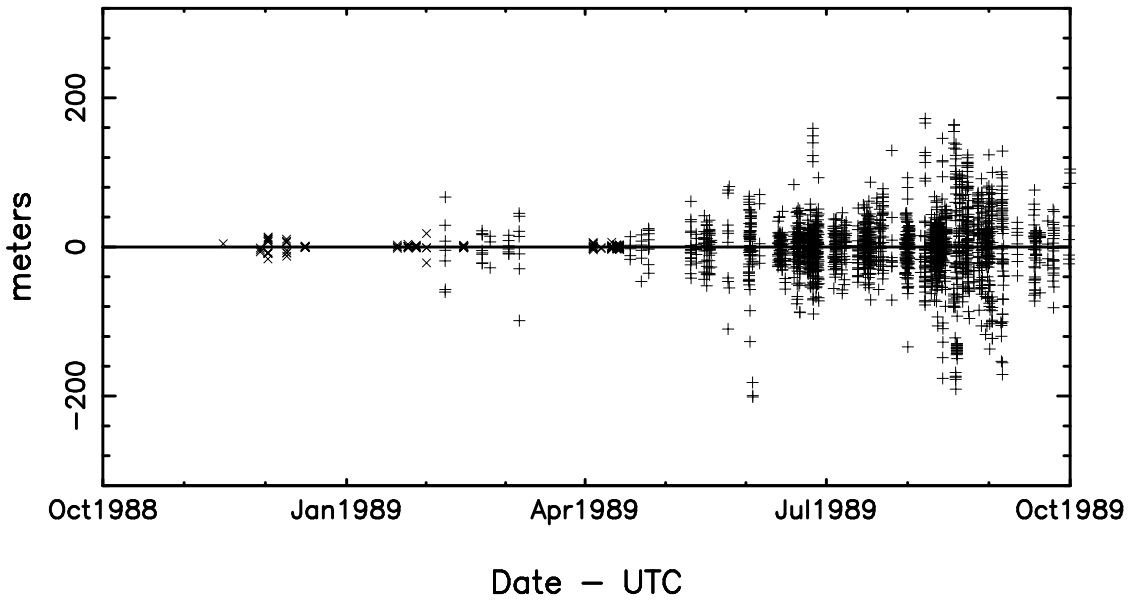

Figure 8. Range Residuals

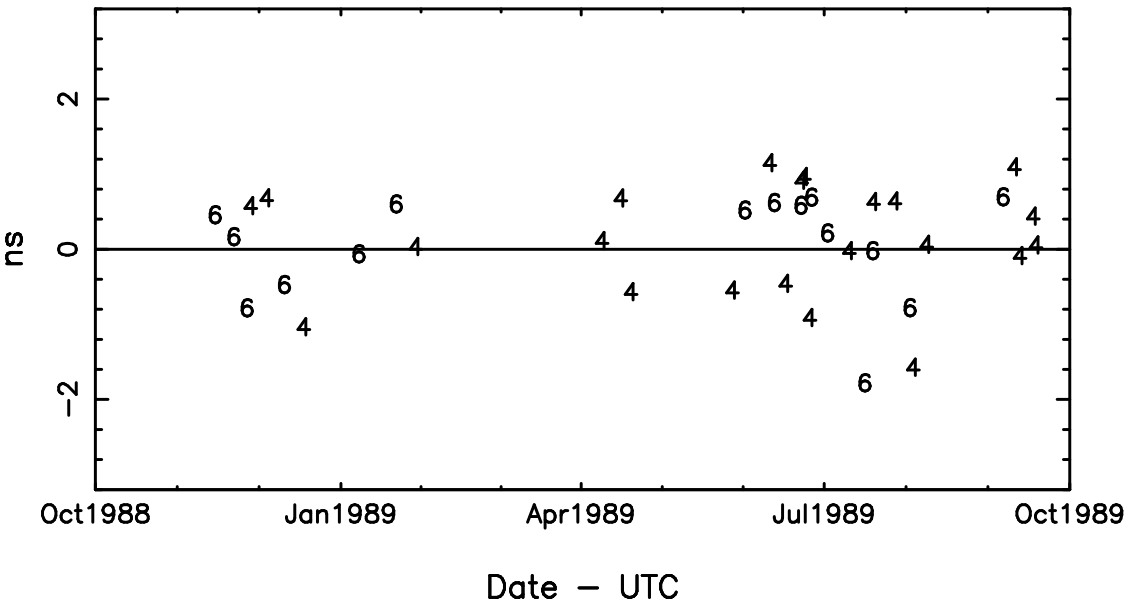

Figure 9. ΔDOR Residuals

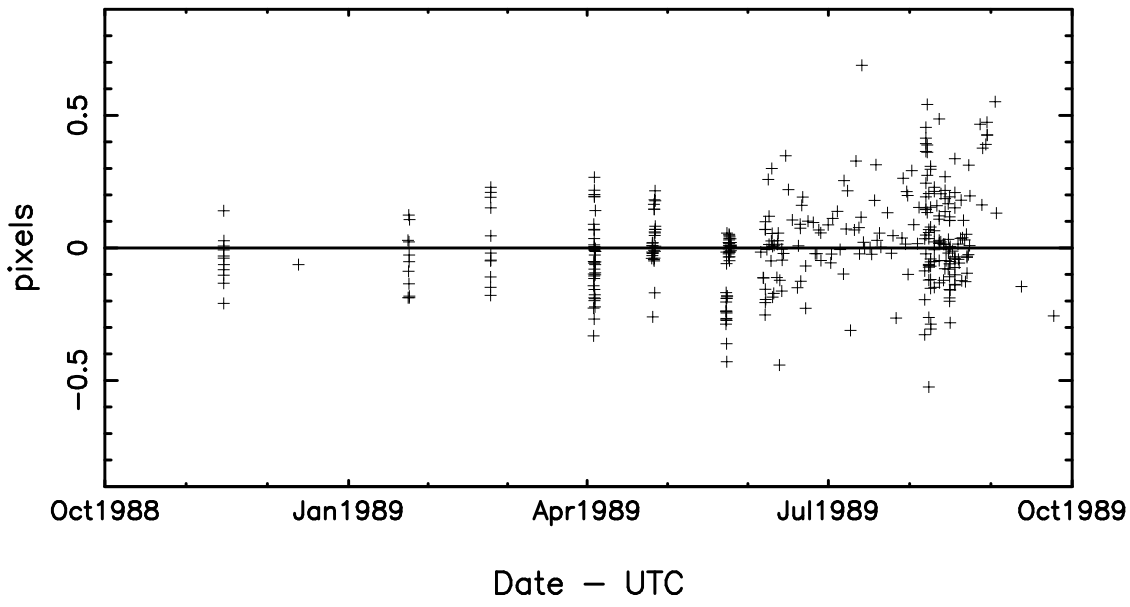

Figure 10. Triton Sample Residuals

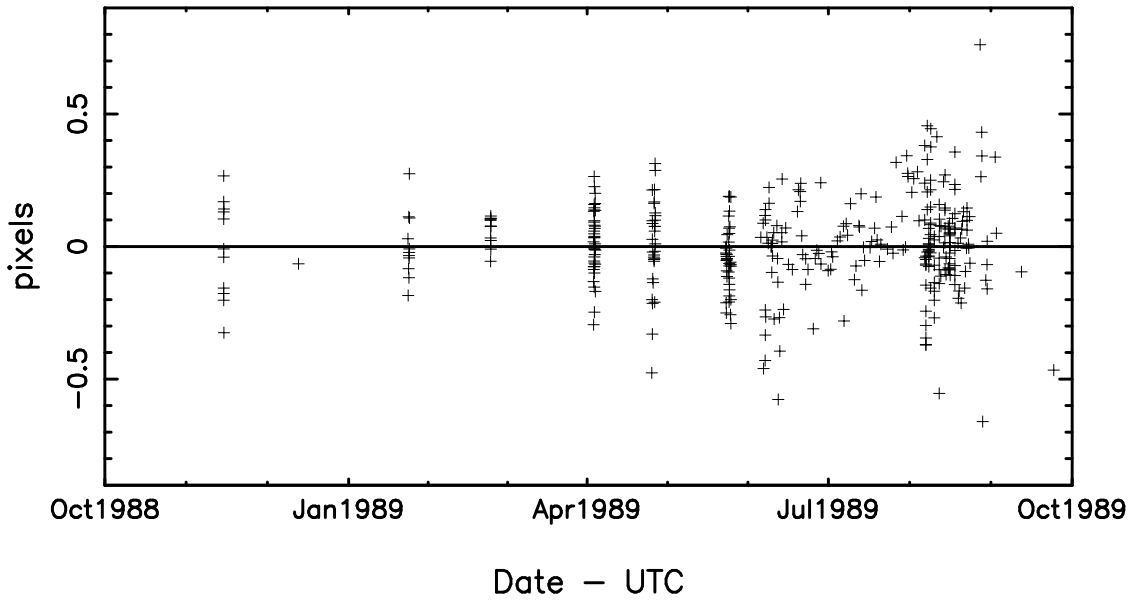

Figure 11. Triton Line Residuals

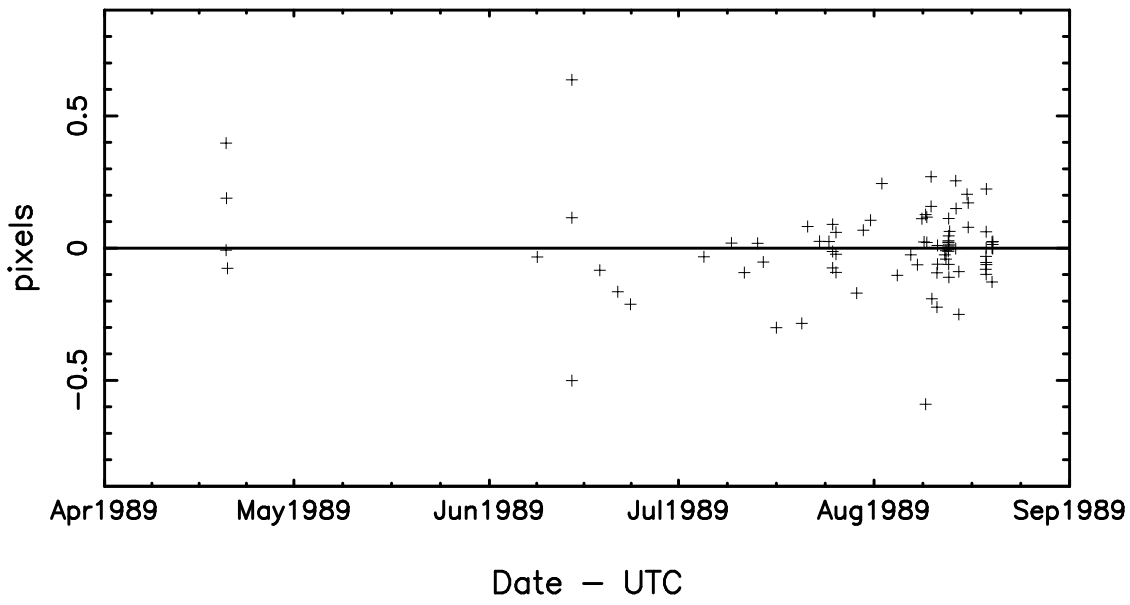

Figure 12. Nereid Sample Residuals

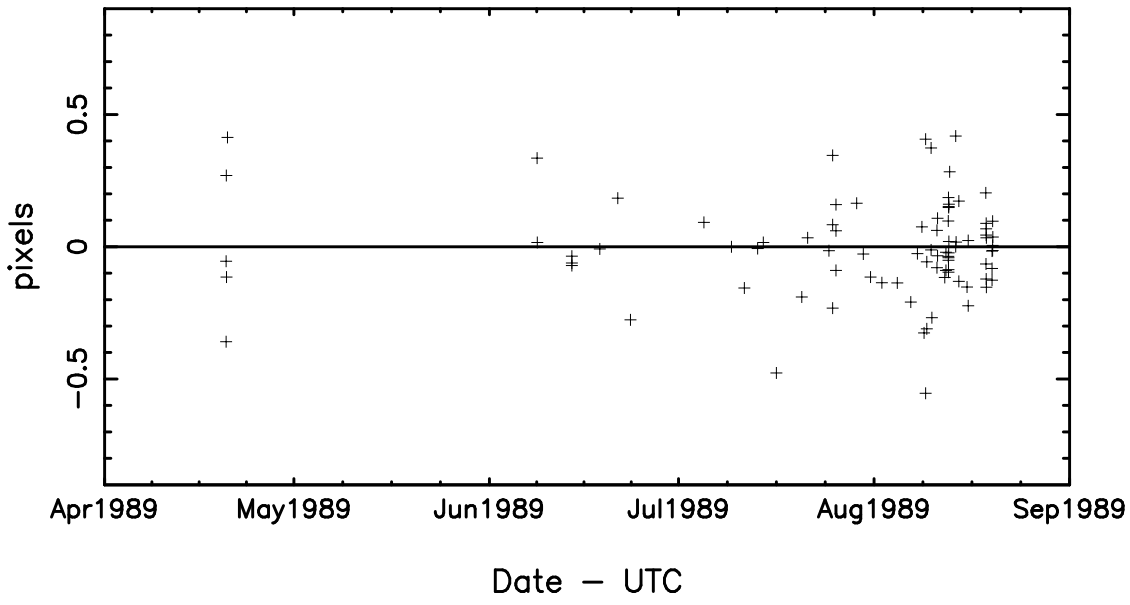

Figure 13. Nereid Line Residuals

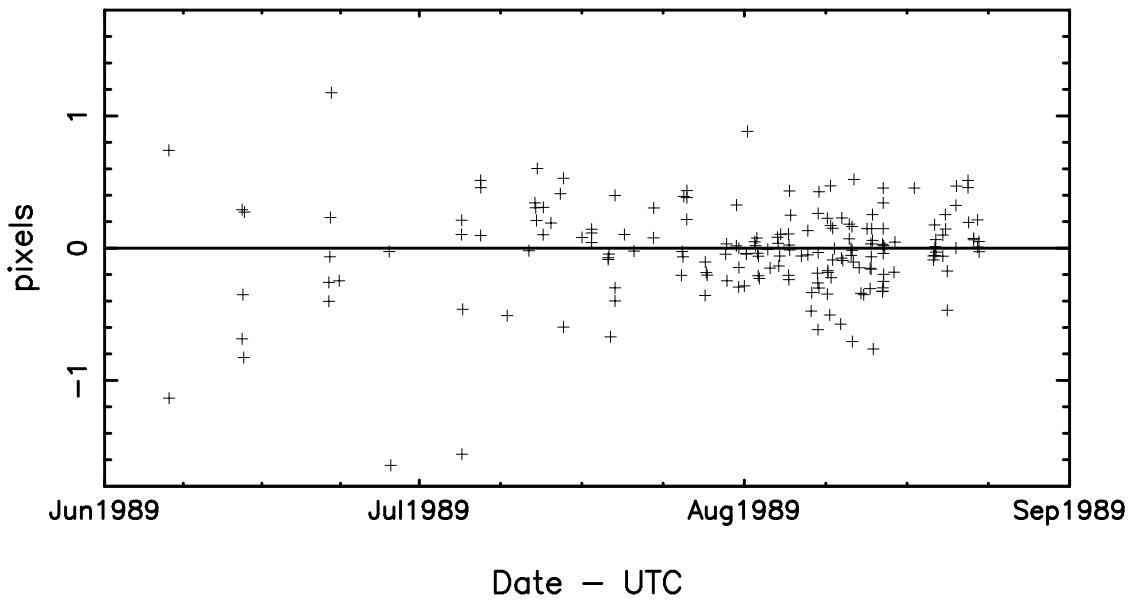

Figure 14. Proteus Sample Residuals

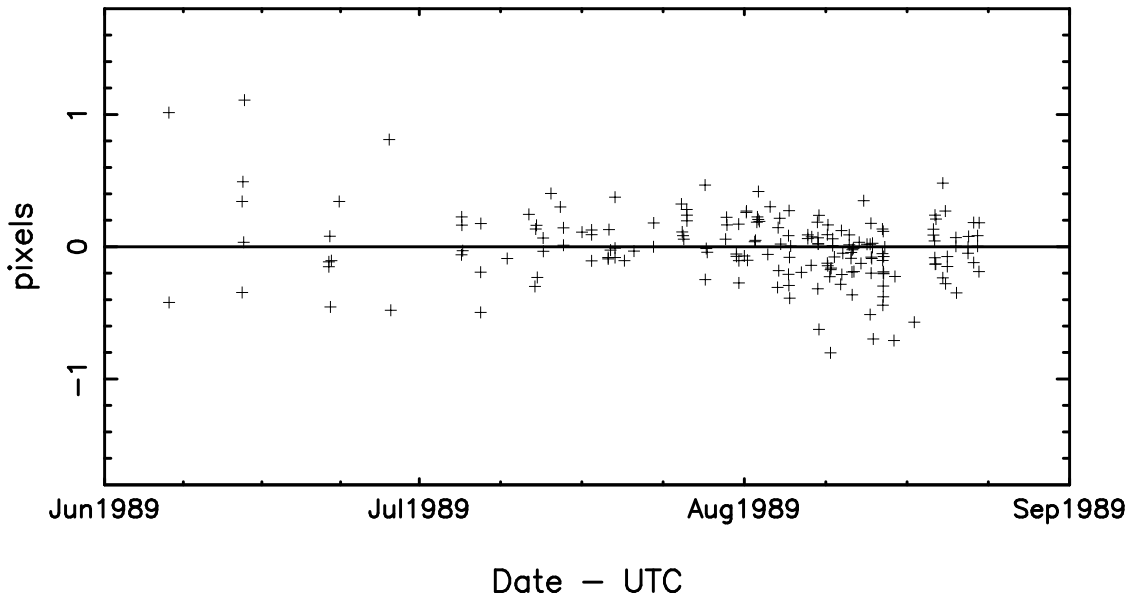

Figure 15. Proteus Line Residuals